Effects of current density on morphology and magnetic properties of Co-TiO_2 electrodeposited nanocomposite films

M. POIANA[a], L. VLAD[a], P. PASCARIU[a], A. V. SANDU[b], V. NICA[a], V. GEORGESCU[a]
[a]*Faculty of Physics, Alexandru Ioan Cuza University of Iasi 700506, Romania*
[b]*"Gheorghe Asachi" Technical University, Iasi*

We describe some experimental results concerning the method of preparation by electrolysis of novel nanostructured magnetic Co-TiO_2 composite films consisting of a cobalt matrix with dispersed titania nanoparticles. The films were electrodeposited onto copper substrates from an acid cobalt sulphate bath containing $CoSO_4 \cdot 7H_2O$, H_3BO_3, NaCl, $Na_2SO_4 \cdot 10H_2O$ and TiO_2 nanoparticles, with continuous magnetic stirring of the bath. The applied current density (varied in the range of 0.011 – 0.032 A/cm^2) significantly influenced the film composition (introducing up to 14.0% TiO_2 as average percentage in the film), the texture and their magnetic properties (magnetic anisotropy, saturation magnetization and coercive field).

(Received January 29, 2012; accepted April 11, 2012)

Keywords: Composite materials, Thin films, Electrodeposition, Magnetic properties, Co-TiO_2 films

1. Introduction

Nanostructured composite materials or nanocomposites are under extensive investigation in modern materials science, due to their interesting properties. Nanocomposite materials encompass a large variety of systems such as one-dimensional, two-dimensional, three-dimensional and amorphous materials, made of distinctly dissimilar components and mixed at the nanometer scale [1 and 2]. Nanocomposite materials can be classified, according to their matrix materials, in three different categories: ceramic matrix nanocomposites, metal matrix nanocomposites and polymer matrix nanocomposites [3]. The most frequent techniques for the processing of metal matrix nanocomposites are: spray pyrolysis, liquid metal infiltration, rapid solidification, vapour techniques (PVD, CVD), electrodeposition and chemical methods, which include colloidal and sol-gel processes [3]. Electrochemical co-deposition is a good technique in the field of nanocomposites in metal matrix because electroplating is a very appropriate and inexpensive method to produce metal coatings. It combines the advantages of metal electroplating with those of composite materials. By electrolysis of plating solutions, in which micron or sub-micron size particles are suspended, it is possible to obtain novel materials with improved and/or combined properties, which make them interesting for different applications such as chemical sensors, magnetic sensors, materials for electrocatalysis and photoelectrocatalysis. Interest in the technique grew, and a better understanding of the process was obtained in recent years. The most recent developments in this field and the overview of the experimental facts reported in the literature concerning electrolytic composite plating have been published in refs. [1, 4 – 6]. Composites containing incorporated TiO_2 particles are interesting materials, due to the semiconducting properties of TiO_2, with applications as photocatalysts, particularly in the treatment of polluted water [7], but, in the same time, due to magnetic properties of Co matrix. Since the discovery of Matsumoto et al. [8], ferromagnetic Co/TiO_2 thin films fabricated by laser molecular beam epitaxy have drawn many researchers attention due to their Curie temperature higher than room temperature. More attention has been focused on ferromagnetism in Co-doped TiO_2 anatase films, nanocrystals, nanorods and nanotubes, with potential applications in spintronics [8 – 14].

In recent years a lot of work has been performed on the TiO_2 co-deposition process with Ni, Cu, Ag and Zn as metallic components [15 – 23]. It was found that the nanocomposite properties are influenced by the deposition parameters, namely current profile, bath composition, *p*H, temperature, and TiO_2 particles concentration in the bath [24]. A few literature references can be found about the incorporation of TiO_2 nanoparticles in ferromagnetic Co matrix; the effect of incorporated TiO_2 on the tribological properties [25], morphology, hardness, and corrosion resistance of coatings [26] was investigated. No work has been reported so far on the magnetic properties of such Co-TiO_2 nanocomposite films.

In this paper we propose a new method for electrodeposition of Co-TiO_2 nanocomposite thin films and we study the effect of current density on the morphology, structure, and magnetic properties of these films, containing different percentage of incorporated TiO_2 particles.

2. Experimental

Electrodeposition of thin films composed of a cobalt metal matrix with included TiO_2 nanoparticles has been carried out in a solution based on cobalt sulphate, containing TiO_2 nanoparticles dispersed in the bath, under magnetic stirring. Analytical reagents and distilled water were used to prepare the plating solution. Prior to plating, the TiO_2 nanoparticles, Degussa (mixture of rutile and anatase), with an average diameter around 28 nm were dispersed in the electrolyte. In a first step, we established the optimum bath composition and parameters of electrolytic deposition for Co-TiO_2 composites films. The electrolyte contains: cobalt sulphate 0.046 M $CoSO_4 \cdot 7H_2O$, boric acid 0.32 M H_3BO_3, some additional substances (NaCl, $Na_2SO_4.10H_2O$) selected according to the deposited layer quality, by preliminary electrodeposition experiments, and a variable quantity (from 0.010M to 0.125M) of titanium dioxide nanoparticles. The temperature of the electrolyte was of (23 ± 1) ^oC, and the rotation speed of the magnetic stirrer was kept constant at 500 rpm. The electrodeposition was carried out under galvanostatic conditions, using a three-electrode cell with a platinum anode, a copper cathode and a quasi-reference electrode of platinum wire. A cfc (100) - textured polycrystalline copper disc, 23.0 mm in diameter, was used as substrate material. It was mounted in a specially designed sample holder which left exposed a 3.14 cm^2 area, with a distance of 2.0 cm between the two electrodes. The anode was a 3.14 cm^2 platinum sheet, and the quasi-reference electrode was a platinum wire having the contact area with the electrochemical solution of 0.06 mm^2. The electrodeposition was generated and controlled by a computer programmable d.c. source.

The crystalline structure of the films was examined by X-ray diffraction (XRD), using a SHIMADZU XRD-6000 powder diffractometer (Cu $K_{\alpha 1}$ radiation, λ = 1.54059 Å). The crystallite size and structure of the electrodeposited Co-TiO_2 nanocomposite films were calculated from XRD analysis. A Vega II LSH Scanning Electron Microscope (SEM) coupled with an energy-dispersive X-ray (EDAX) system of Quantax QX2 type was used for morphological analysis and composition determination of the films.

The hysteresis loops measurements of the films were performed using an a.c. induction type device with computerized data acquisition system (at a frequency of 50 Hz, in a 60 kA/m maximum field applied in the plane of the samples, at room temperature). In addition, a torque magnetometer (H_{max}=95 kA/m) was used to measure anisotropy and torque curves of the samples, at room temperature.

3. Results and discussion

3.1. Electrodeposition of Co–TiO_2 nanocomposite thin films

The study of electrodeposition processes was performed by voltammetry in the working cell. Fig. 1a shows the current density versus applied voltage (U_{bias}) curves (called cathodic polarization curves or voltammograms), obtained for three different electrolytic solutions (labelled 1, 2 and 3) with various concentrations of TiO_2 (0.010 M, 0.035 M and 0.125 M, respectively). These curves were recorded at 0.3 mV/s sweep rate. The same curves for the solution containing 0.035 M TiO_2 nanoparticles are presented in Fig. 1b. Voltammograms were drawn upward by changing the bias voltage from 0.000 V to -5.000 V and backward from -5.000 V to 0.000 V, and the curves were marked with arrows, correspondingly. Fig. 1a shows that the current density (for a bias voltage of 5.000 V) decreases in absolute value from 0.080 A/cm^2 to 0.048 A/cm^2 with increasing concentration of TiO_2 nanoparticles in solution (from 0.010M to 0.125M, respectively). The observed slight decrease in the current density, in the presence of the TiO_2 nanoparticles, indicates that the TiO_2 nanoparticles do no promote the cobalt deposition. It can be assumed that the decrease in the current density is due to the adsorption of the TiO_2 particles on the cathode surface, which would lead to a worse surface area.

The voltammograms from Fig. 1b display very similar behaviour on the two branches (with increasing and decreasing the absolute value of cathode potential), which is characteristic to close to equilibrium thermodynamic processes. The Co ions discharge potential measured versus reference electrode is to a certain extent influenced by the presence of TiO_2 in solution, showing the values of: 0.63 V, 0.67 V and 0.68 V, for the solutions 1, 2 and 3, respectively.

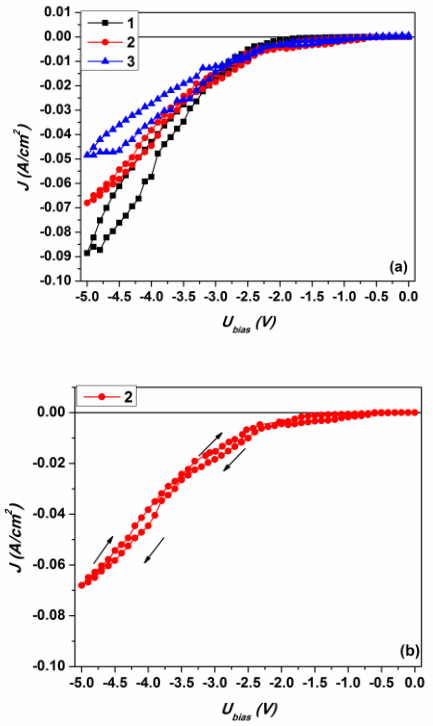

Fig. 1. Current density versus bias voltage curves, for solutions with different concentrations of TiO_2: a) 0.010M (1), 0.035M (2) and 0.125M (3) and b) detailed view of the curve recorded for the solution (2), containing 0.035M TiO_2.

The electrodeposited films show the best quality (from the point of view of uniformity and adherence to the support) when they are prepared from the solution 2. Consequently, we prepared the samples studied in this work by using the solution labelled 2, containing: 0.046 M $CoSO_4 \cdot 7H_2O$, 0.32 M H_3BO_3, 0.035M TiO_2 nanoparticles, and 0.44 M NaCl, 0.035 M $Na_2SO_4.10H_2O$ as additional substances. All the studied samples were prepared with the same electrical charge passing through electrolyte (≈ 50.62 C); as a result, they have about the same average thickness, of about 2.85 μm.

3.2. Morphological and structural analysis of electrodeposited Co-TiO_2 nanocomposite films

In order to evaluate the effect of current density on microstructure and properties of Co-TiO_2 nanocomposite films, we deposited, in galvanostatic regime, a series of films from the solution 2, by using various values of current density. We selected as representative some films deposited at the current densities of 0.032 A/cm^2, 0.026 A/cm^2, 0.022 A/cm^2 and 0.011 A/cm^2; these samples were labelled as A1, A2, A3 and A4, respectively, and they will be characterized in the following part of the paper.

We found that the current density exhibits a strong influence both on the TiO_2 content and on surface morphology of the nanocomposite films, performed by SEM experiments. The TiO_2 presence in the nanocomposite films was determined by EDAX study. The EDAX spectrum of the Co-TiO_2 nanocomposite film electrodeposited at 0.032 A/cm^2 is shown in Figure 2. The peaks of Co, Ti and O can be clearly seen in this figure, indicating that the film contains the Ti, Co and O elements. The presence of Cu line may be ascribed to the substrate of the nanocomposite films. The analysis gives the average elemental percentage of Ti (as TiO_2) and Co, of 14.0% and 86.0%, respectively. Therefore, it is confirmed the presence of TiO_2 nanoparticles incorporated in the cobalt matrix.

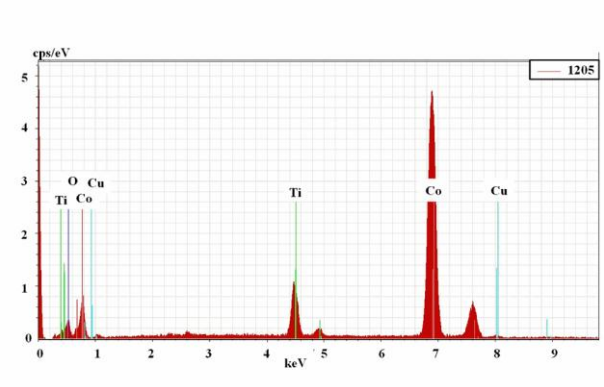

Fig. 2. EDAX spectrum of Co-TiO_2 nanocomposite film electrodeposited at 0.032 A/cm^2 on Cu (100) substrate (0.035 M TiO_2 in the plating bath).

The incorporated TiO_2 particles content in nanocomposite films as a function of current density is shown in Fig. 3. Due to the limited number of the samples, the line should be considered only as a guide to the eyes. As it can be seen in this figure, the highest content of TiO_2 in the nanocomposite films was obtained from the current density of 0.032 A/cm^2. We suppose that at a low down current density (0.022 A/cm^2) cobalt ions move slowly, and the adsorption process is not promoted. As a result, volume content of the particles will be low in such films. By applying the current density of 0.026 A/cm^2, mobility of cobalt ions increases and the films contain more TiO_2 nanoparticles. The enhancement of current density up to 0.032 A/cm^2 increases the quantity of TiO_2 in film as a result of faster transport of cobalt ions.

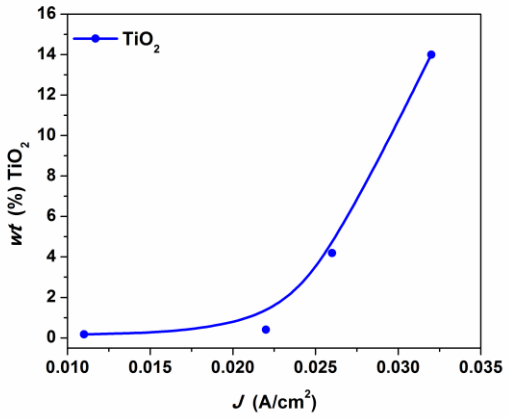

Fig. 3. The content of TiO_2 nanoparticles as a function of the current density, in the films electrodeposited from the solution 2 (containing 0.035 M TiO_2 nanoparticles).

The surface morphology of the samples A1, A2, A3 and A4, analyzed by SEM is presented in Fig. 4 (a – h) at two length scales: 6 μm (a, c, e, g) and 100 μm (b, d, f, h). The Co grains are grown from different nucleation sites onto the Cu substrate by a Volmer-Weber insular grain growth mechanism, and they tend to form conglomerates, especially in the case of the samples A1 and A2 [Figs. 4(a - d)], obtained at 0.032 A/cm^2 and 0.026 A/cm^2, respectively.

By incorporation of TiO_2 in the films, the surface morphology of the nanocomposite samples is gradually changed. By increasing the current density, starting from the bottom images (Fig. 4 g, h) to the top ones (Fig. 4 a, b), the morphology of the films is completely changed to cauliflower with pyramid shapes in around. The same type of morphology was obtained by S. Sanjabi and A. Shirani [26] for electrodeposited Co-TiO_2 coatings. Because the cathode surface is covered partially by TiO_2 nonconductive nanoparticles, the current density is increased locally leading to increasing the cobalt nucleation on preferred sites. Thus, the cobalt crystals are nucleated and grown in the shape of cauliflower and wide pyramid in the coatings. By increasing the current density, the cauliflower size became larger and the pyramid shapes became larger (Fig. 4 a, b).

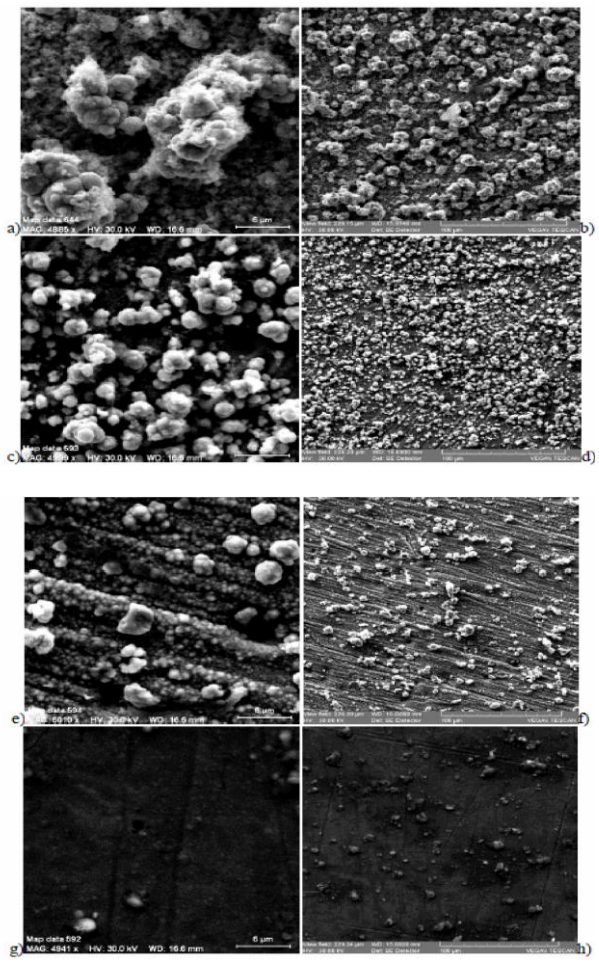

Fig. 4. SEM micrographs of Co–TiO_2 nanocomposite films electrodeposited at the current densities of: 0.032 A/cm^2 (a, b), 0.026 A/cm^2 (c, d), 0.022 A/cm^2 (e, f) and 0.011 A/cm^2 (g, h). Scale bar is 6 μm (for the left column) and 100 μm (in the right column).

The codeposition mechanism of TiO_2 nanoparticles on the cathode surface could be explained by Guglielmi's two-step adsorption model [1, 27, 28]. In the first step, which is of a physical nature, particles approaching the cathode become loosely adsorbed on the cathode surface. These loosely adsorbed particles are still surrounded by a cloud of adsorbed ions. In the second step the particles lose this ionic cloud and become strongly adsorbed on the cathode. This step is thought to be of an electrochemical character, that is, it depends on the electric field at the cathode. Finally, the strongly adsorbed particles are occluded by the growing metal layer.

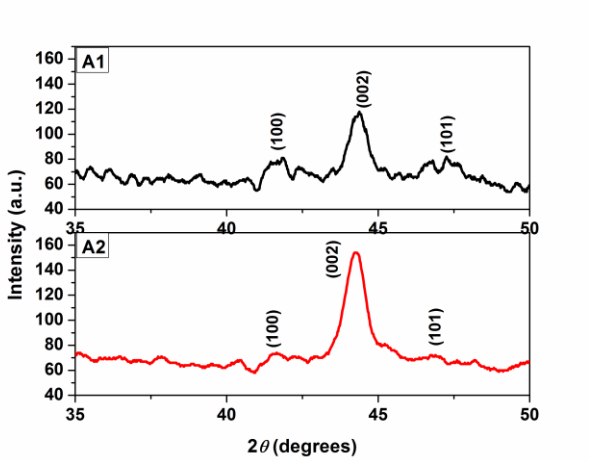

Fig. 5. XRD patterns (enlargement for the region of Co lines) of the A1 (0.032 A/cm^2) and A2 (0.026 A/cm^2) nanocomposite samples.

Fig. 5 shows the X-ray diffraction (XRD) patterns for the region of Co lines of the A1 (0.032 A/cm^2) and A2 (0.026 A/cm^2) nanocomposite samples. The peaks for Co appear at $2\theta = 41.82°$, $2\theta = 44.38°$, and $2\theta = 47.28°$, which are well indexed to the crystal planes of hcp-Co (100), (002), and (101), respectively. We determined the average crystallite diameter (*ACD*) of the Co particles from the major diffraction peak (002) using the Debye-Scherrer's formula:

$$ACD = \frac{0.9\lambda}{(\Delta w \times \cos\theta)}, \quad (1)$$

where λ is the X-ray wavelength, θ is the angle of Bragg diffraction peak, and Δw is its full width at half maximum (FWHM) in radians, and 0.9 signifies the instrumental broadening. The calculated *ACD* value of nanocrystalline Co is found to be about 12 nm for the sample A1 (electrodeposited at current density 0.032 A/cm^2) and 11 nm for the sample A2 (0.026A/cm^2). There was no significant intensity of TiO_2 peaks in the XRD patterns of these samples, possibly due to very low amount of TiO_2 nanoparticles in composite films. However, the EDAX study certifies the existence of TiO_2 particles in the composite film (14.0 wt% and 4.2 wt % for the samples A1 and A2, respectively). From the diffraction patterns (Fig. 5), the cell parameters of the hexagonal structures were calculated. We have found the following values for cell parameters, a=2.49 Å and c=4.08 Å.

Careful observation of Fig. 5 reveals different relative peak intensities corresponding to different planes of cobalt with change in electrodeposition current density. For the study of the texturing, the relative texture coefficient (*RTC*) of each plane for the examined samples was calculated using the following equation [16, 17, 29]:

$$RTC_{(hkl)} = \frac{I_{s(hkl)}/I_{p(hkl)}}{\sum\left(I_{s(hkl)}/I_{p(hkl)}\right)} \times 100, \quad (2)$$

where $I_{s(hkl)}$ and $I_{p(hkl)}$ are the diffraction intensities of the (h k l) plane measured in the diffractogram for the film and the standard Co powder sample (JCPDS no. 01-1278), respectively. Table 2 shows the average crystallite diameter and *RTC* data calculated on three different planes, i.e. (100), (002), and (101) for the studied samples.

Table 1. Effect of current density on average crystallite diameter and the relative texture coefficient for electrodeposited A1 and A2 nanocomposite films.

Sample/Current density (A/cm^2)	*ACD* (nm)	texture (*RTC*)	Relative coefficient	
		(100)	(002)	(101)
A1/0.032			38.8	17.0
	12	4.2		
A2/0.026			47.9	13.9
	11	8.2		

The analysis of diffractograms shows that the current density in the plating bath has a strong influence on the crystal orientation in the deposited film, even if the change in grain size is not noticeable. Thus, the Co (100) and (101) diffraction peak intensities in the composite films decrease, while the (002) peak increases, when the current density decreases. These results suggest that the particles embedded in the electrodeposited films can affect the preferred orientation of the metal matrix as a consequence of changes on the metal deposition mechanism; these results are in accordance with those stated in the literature for the Ni/TiO_2 nanocomposite coatings [16, 17, 29].

3.2. Magnetic characterization of Co-TiO_2 nanocomposite films

The hysteresis loops, obtained at room temperature by using an a.c. induction type device with computerized data acquisition system, in a 60 kA/m maximum field applied in the plane of the samples, are shown in Fig. 6. We have found that the increase of current density, causing the increase of TiO_2 particles content in the film, completely changes the magnetic properties of the sample. Fig. 6 shows a comparison between hysteresis loops of nanocomposite films A1, A2, A3 and A4 electrodeposited at the current density values of 0.032 A/cm^2, 0.026 A/cm^2, 0.022 A/cm^2 and 0.011 A/cm^2, respectively. We have found that, by keeping the concentration of TiO_2 constant in electrolytic bath, the magnetic behaviour of the electrodeposited samples is much influenced by the current density values. We consider here that coercivity (H_c) and saturation magnetization (M_s) are the values measured from the hysteresis loops in these experiments (although this is not the saturation field for all the samples). From the Figs. 6 and 7 it can be seen that the shape of the loops and the coercivity differ significantly together with the current density (hence the TiO_2 content of the nanocomposite films is increased).

Saturation magnetization and coercive field for the samples A1 – A4 as a function of the electrodeposition current density are shown in Fig. 7. Saturation magnetization decreases with increasing current density, which may be due to the inclusion of a larger amount of TiO_2 in nanocomposite thin film. The variation in coercive fields with current density is much less pronounced than that for the saturation magnetization. The increase in cauliflower grain size with increasing current density is thought to be a possible cause of the reduction in coercivity, implying that the energy barriers to domain wall motion are easier to overcome. The increase in the coercive fields for low current density deposited films could be a consequence of the formation of small crystallites which act as strong domain wall pinning sites. The increase in coercivity revealed in Fig. 6 is consistent with the changes in the microstructure of the films, emphasized by SEM micrographs (Fig. 4).

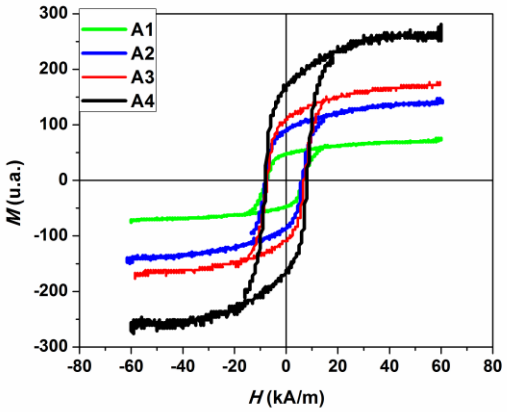

Fig. 6. Comparison between hysteresis loops recorded for the samples A1, A2, A3 and A4.

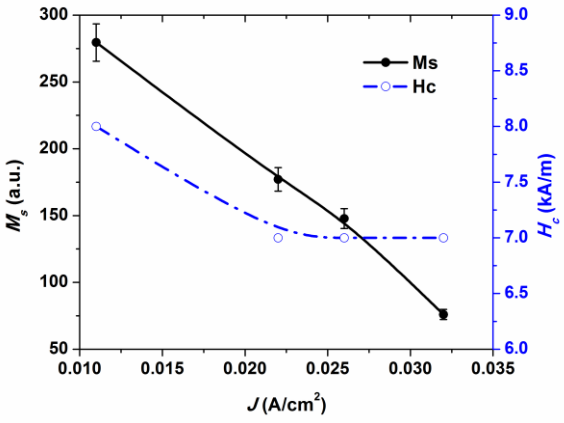

Fig. 7. Saturation magnetization (M_s) and coercive field (H_c) for the samples A1–A4 as a function of the electrodeposition current density.

The magnetic anisotropy of the Co-TiO_2 magnetic nanocomposite films was measured at room temperature with a torque magnetometer. Torque L on the samples is

recorded as a function of the angle (θ) between the plane of the film and the applied magnetic field H. The film plane was oriented perpendicularly to the field-rotation plane, e. g. the torque was measured around an arbitrary axis parallel to the film plane, starting from the plane of the film ($\theta = 0$). Fig. 8 (a) shows the static torque curves for the samples A1, A2 and A4, performed for clockwise and anticlockwise rotation of a 28 kA/m magnetic field. In Fig. 8 (a), the curves labelled F correspond to a clockwise rotation of the magnetic field and those labelled B correspond to anticlockwise rotation. The experimental torque curves exhibit mainly a twofold symmetry (the torque is proportional to sin 2θ), with a positive slope at $\theta = 0^o$. The preferred direction of magnetization or easy axis of magnetization can be seen in torsion magnetometer curves as the points matching to L=0, corresponding to the free energy minima [30, 31]. The peaks in the torsion magnetometer curves correspond to the unfavourable or hard axis of magnetization.

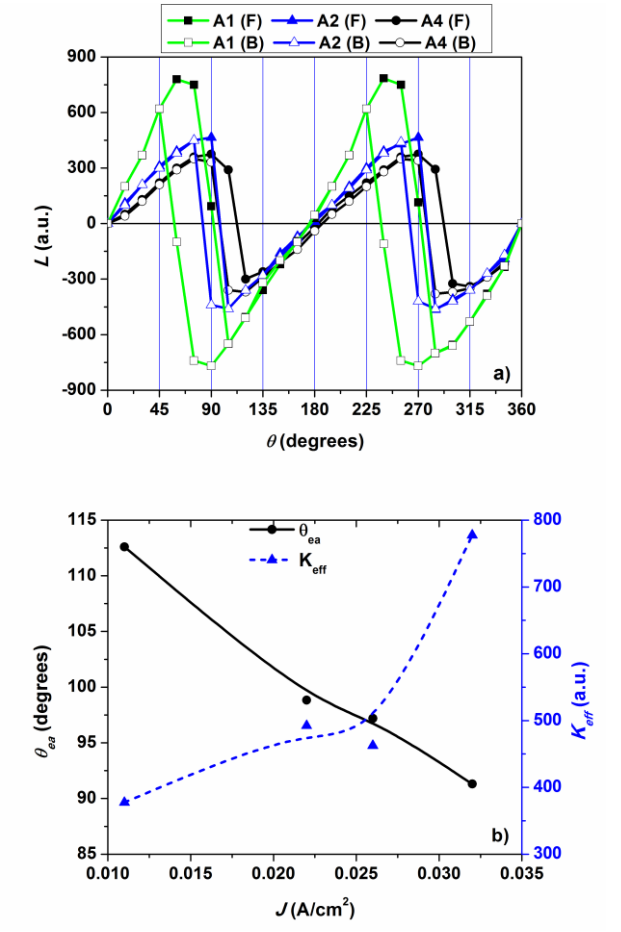

*Fig. 8. a) Magnetometer torque curves for the samples A1, A2, and A4 plotted for clockwise rotation, from 0° to 360° (**F**) and anticlockwise rotation, from 360° to 0° (**B**). The torque curves were measured in the field of 28 kA/m. b) The angle θ_{ea} between the easy axis of magnetization and the film plane, and the effective anisotropy constant, K_{eff}, as a function of the deposition current density, for the same samples.*

When the applied field increases, exceeding the anisotropy field, the torque curves (F and B) become asymmetric, i.e. the rotational losses appear and they are measurable from the area enclosed by clockwise and anticlockwise curves. For fields exceeding the anisotropy field, the torque curves (F and B) are irreversible.

The effective magnetic anisotropy K_{eff} (in arbitrary units) is estimated from the maximum value of the torque (L_{max}) in the applied magnetic field. It has to be mentioned that K_{eff} is not the same as the intrinsic magnetic anisotropy K_u that is the quantity defined as the field goes to infinity. Furthermore, K_u is the uniaxial anisotropy (with twofold symmetry), whereas K_{eff} is the magnetic anisotropy including the higher order symmetry and the shape anisotropy. The measured K_{eff} and the angle θ_{ea} between the easy axis of magnetization and the film plane as function of current density are shown in Fig. 8 (b), for the samples A1 – A4. The lines are drawn to guide the eyes.

Taking into account that K_{eff} is estimated from the following equation

$$K_{eff} = L_{\max} = K_u - 2\pi M_s^2, \qquad (3)$$

the decrease of M_s (as it is shown in Figs. 6 and 7) while the current density is increased could explain partially the shape of the K_{eff} (J) curve from Fig. 8 (b). Another contribution to diminish M_s could be due to the decreasing value of uniaxial anisotropy (expressed by increase of θ_{ea}) when the texture and morphology of the samples are modified by increasing current density.

4. Conclusions

We demonstrate in this work that it is feasible to prepare Co-TiO_2 nanocomposite films by properly incorporating the TiO_2 nanoparticles to be co-deposited in the Co plating bath. The concentration of co-deposited TiO_2 nanoparticles in the composite films was controlled by current density. The co-deposited TiO_2 nanoparticles significantly affect the morphology of the film. The EDAX spectra revealed the presence of Ti in the electrodeposited film, in addition to an increase of the oxygen content, indicating the inclusion of TiO_2 nanoparticles in the cobalt matrix. The surface morphology as well as the texture of the cobalt matrix is significantly changed due to the addition of titania particles in the film. The TiO_2 nanoparticles embedded in the electrodeposited films affect the preferred orientation of the metallic matrix, as a consequence of changes on the metal deposition mechanism.

The saturation magnetization and the hysteresis loops shapes modify as a function of film microstructure, changed by the current density control. As a consequence of the increase in current density, the TiO_2 content in the films increases and this has an important influence on the magnetic properties of the films. The values of coercive field varied in the range H_c = (7.0 – 8.0) kA.m^{-1}. The inclusion of TiO_2 in a nanocomposite layer with increasing

current density causes the decrease of saturation magnetization from 279.5 (a.u.) to 76.0 (a.u). Magnetic anisotropy of nanocomposite films depends on the concentration of TiO_2. The angle θ_{ea} between the easy magnetization axis and the film plane exhibits values between 91.3 degrees and 112.6 degrees (for films deposited at 0.032 A/cm^2 and 0.011 A/cm^2, respectively), due to different texture of the films.

Acknowledgements

This work was partially supported by the European Social Fund in Romania, under the responsibility of the Managing Authority for the Sectoral Operational Programme for Human Resources Development 2007-2013 [grants POSDRU/88/1.5/S/47646 and POSDRU/89/1.5/S/49944]. The authors would like to acknowledge Professor Ioan Sandu from the "Alexandru Ioan Cuza" University for his help with the SEM experiments.

References

[1] A. Hovestad, L. J. J. Janssen, J. Appl. Electrochem **25,** 519 (1995).
[2] M. Schlesinger, M. Paunovic, Modern Electroplating, Fourth Edition, John Wiley & Sons Inc., (2001).
[3] P. H. C. Camargo, K. G. Satyanarayana, F. Wypych, Materials Research **12**, 1 (2009).
[4] J. P. Celis, J. R. Roos, C. Buelens, J. Fransaer, Trans. Inst. Met. Finish. **69**, 133 (1991).
[5] C. Buelens, J. Fransaer, J. P. Celis, J. R. Roos, Bull. Electrochem. **8**, 371 (1992).
[6] J. Fransaer, J. P. Celis, J. R. Roos, Met. Finish. **91**, 97 (1993).
[7] A. Fujishima, T. N. Rao, D. A. Tryk, J. Photochem Photobiol C: Photochem Rev **1**, 1 (2000).
[8] Y. Matsumoto, M. Murakami, T. Shono, et al., Science **291**, 854 (2001).
[9] S. A. Chambers, T. Droubay, C. M. Wang, A. S. Lea, R. F. C. Farrow, L. Folks, V. Deline, S. Anders, Appl. Phys. Lett. **82**, 1257 (2003).
[10] J. D. Bryan, S. A. Santangelo, S. C. Keveren, D. R. Gamelin, J. Am. Chem. Soc. **127**, 15568 (2005).
[11] D. Wu, Y. F. Chen, J. Liu, X. N. Zhao, A. D. Li, N. B. Ming, Appl. Phys. Lett. **87**, 112501 (2005).
[12] X. G. Xu, X. Ding, Q. Chen, L. M. Peng, Phys. Rev. B **73**, 165403 (2006).
[13] C. Huang, X. Liu, L. Kong, W. Lan, Q. Su, Y. Wang, Appl. Phys. A: Mater. Sci. Process. **87**, 781 (2007).
[14] X. W. Wang, X. P. Gao, G. R. Li, L. Gao, T. Y. Yan, H. Y. Zhub, Appl. Phys. Lett. **91**, 143102 (2007).
[15] H. Simunkova, P. Pessenda-Garcia, J. Wosik, P. Angerer, H. Kronberger, G. E. Nauer, Surf. Coat. Tech. **203**, 1806 (2009).
[16] S. Spanou, E.A. Pavlatou, N. Spyrellis, Electrochim. Acta **54**, 2547 (2009).
[17] D. Thiemig, A. Bund, Surf. Coat. Tech. **202**, 2976 (2008).
[18] M. S. Ali Eltoum, A. M. Baraka, M. Saber M., ELfatih A. Hassan, International Journal of Multidisciplinary Science and Engineering (IJMSE) **2**, 1 (2011).
[19] S. A. Lajevardi, T. Shahrabi, V. Hasannaeimi, Mater. Corros. **62**, 29 (2011).
[20] S. Ramalingam, V. S. Muralidharan, A. Subramania, J. Solid State Electrochem. **13**, 1777 (2009).
[21] J. Fustes, A. Gomes, M. I. da Silva Pereira, J. Solid State Electrochem. **12**, 1435 (2008).
[22] D. E. Rusu, P. Cojocaru, L. Magagnin, C. Gheorghies, G. Cârâc, J. Optoelectron. Adv. Mater. **12**, 2419 (2010).
[23] D. Blejan, D. Bogdan, M. Pop, A. V. Pop, L. M. Muresan, Optoelectron. Adv. Mater. Rapid Commun. **5**, 25 (2011).
[24] T. Deguchi, K. Imai, H. Matsui, M. Iwasaki, H. Tada, S. Ito, J. Mater. Sci. **36**, 4723 (2001).
[25] E. P. Rajiv, S. K. Seshadri, J. Mater. Sci. **28**, 1758 (1993).
[26] S. Sanjabi, A. Shirani, Mater. Corros. **62**, 1 (2011).
[27] N. Guglielmi, J. Electrochem Soc. **119**, 1009 (1972).
[28] B. Szczygiel, M. Kotodziej, Trans. Inst. Met. Finish **83**, 181 (2005).
[29] S. A. Lajevardi, T. Shahrabi, Appl. Surf. Sci. **256**, 6775 (2010).
[30] M. Daub, F. M. Tufescu, V. Georgescu, J. Optoelectron. Adv. Mater. **8**, 1004 (2006).
[31] D. Pinzaru, S. I. Tanase, P. Pascariu, A. V. Sandu, V. Nica, V. Georgescu, Optoelectron. Adv. Mater. – Rapid Commun. **5,** 235 (2011).

*Corresponding author: violeta.georgescu@uaic.ro